# RIGOROUS FORMULATIONS OF THE THREE-DIMENSIONAL FINITE-DIFFERENCE TIME-DOMAIN METHOD IN SPHERICAL COORDINATES

# การสร้างสูตรโดยละเอียดของวิธีผลต่างสืบเนื่องเชิงเวลาสามมิติในพิกัดทรงกลม


Ekajit Khoomwong
เอกจิต คุ้มวงศ์

Chuwong Phongcharoenpanich
ชูวงค์ พงศ์เจริญพาณิชย์

Monai Krairiksh
โมไนย ไกรฤกษ์

Faculty of Engineering and
Research Center for Communications and Information Technology
King Mongkut's Institute of Technology Ladkrabang
คณะวิศวกรรมศาสตร์และสำนักวิจัยการสื่อสารและเทคโนโลยีสารสนเทศ
สถาบันเทคโนโลยีพระจอมเกล้าเจ้าคุณทหารลาดกระบัง



(ได้รับเมื่อ มีนาคม 2541)

## ABSTRACT

*This paper presents rigorous formulations of the three-dimensional finite-difference time-domain (3D FD-TD) method in spherical coordinates. The finite-difference equations are formulated from Maxwell's equations. The singularities of the space grid in each direction of the spherical coordinates are considered. Then, some alternative radiation boundary conditions (RBCs) are derived and effects of their simulation in calculating field unknowns are illustrated. The stability criterion and time step are also determined. Finally, numerical results of FD-TD algorithm due to various types of applied sources such as pulse and continuous waves are demonstrated.*

## บทคัดย่อ

บทความนี้นำเสนอการสร้างสูตรโดยละเอียดของวิธีผลต่างสืบเนื่องเชิงเวลาสามมิติในพิกัดทรงกลม โดยสมการแมกซ์เวลล์จะถูกแปลงให้อยู่ในรูปผลต่างสืบเนื่อง รวมทั้งได้พิจารณาจุดเอกฐานของการคำนวณในแต่ละทิศทางด้วย จากนั้นได้นำเสนอแนวทางในการหาเงื่อนไขขอบเขตของการแพร่กระจายคลื่น และแสดงผลของเงื่อนไขขอบเขตนั้นต่อการคำนวณค่าสนามที่ไม่ทราบค่า การหาค่าเกณฑ์เสถียรภาพและขั้นเวลาในการคำนวณ และแสดงตัวอย่างผลเฉลยเชิงเลขของวิธีผลต่างสืบเนื่องเชิงเวลาในกรณีที่แหล่งกำเนิดเป็นคลื่นพัลส์และคลื่นต่อเนื่อง


## INTRODUCTION

For about three decades, the FD-TD method has been being advanced its applications by many researchers who interested and believed in it. Yee[9] the pioneer, introduced the ideas of using numerical finite-difference approximations for solving Maxwell's equations in rectangular coordinates. After that, many explorers have conducted advancements in this method. Taflove is the dominant one who

substantiated the FD-TD method by improving the stability criterion formulations[6] and applying this method to analyze several problems[5, 8]. Also, Holland has extended this method to consider the problem in three dimension which is referred to as THREDE code[2, 3]. However, for the analysis of problems involving the spherical configurations, the FD-TD equations must be formulated in spherical coordinates. Holland proposed the so-called THREDS[4] to achieve the FD-TD equations in spherical coordinates. Unfortunately, in Holland's presentation the detail of derivation has not been explained. In addition, the most important thing in FD-TD calculations, the stability criterion, was missing in that considerations.

To complete the derivation, the authors present the rigorous formulations of the 3D FD-TD method in spherical coordinates. The results of the analysis are comprised of FD-TD equations which are constructed from Maxwell's equations, the treatment of singularities, some alternatives easy to implement radiation boundary conditions, behaviors of FD-TD algorithm due to various types of applied sources such as pulse and continuous waves are compared, stability criterion and time step are also determined.

## THREDS Formulations

THREDS is a FD-TD algorithm in three-dimensional spherical coordinates which the electromagnetic pulse (EMP) is applied. This algorithm has two advantages over the algorithm utilizing simple cubical cells in rectangular coordinates. Firstly, because of its spherical geometry so sources can be easily apply to, or detect, field components at any subdivided mesh points by directly referring to these points by using the three orthogonal variables in spherical coordinates. On the other hand, if the rectangular coordinates are chosen, some intricate coordinate transformations are needed. Secondly, if the whole spherical volume is implemented, the only one surface (the outermost) has to be treated by means of RBCs, whereas in rectangular coordinates RBCs are needed to be apply to all of the six surfaces. By these ways, the 3D FD-TD formulations will be started to construct in spherical coordinates, which geometry of the problem is

shown in Figure 1a, from Maxwell's equations in differential or point form with no impressed magnetic current density.

$$\nabla \times \overline{E} = -\frac{\partial \overline{B}}{\partial t}, \tag{1a}$$

and

$$\nabla \times \overline{H} = \overline{J}_i + \overline{J}_c + \frac{\partial \overline{D}}{\partial t}, \tag{1b}$$

where $\overline{E}$, $\overline{H}$ are electric and magnetic field intensities. $\overline{D}$, $\overline{B}$ are electric and magnetic flux densities. $\overline{J}_i$, $\overline{J}_c$ are impressed and conduction electric current densities, respectively. Additionally, for linear, isotropic nondispersive medium, $\overline{B}$ and $\overline{D}$ are related to $\overline{H}$ and $\overline{E}$, respectively, by simple constitutive relations as

$$\overline{B} = \mu \overline{H}, \tag{2a}$$

and

$$\overline{D} = \varepsilon \overline{E}, \tag{2b}$$

where $\mu$ and $\varepsilon$ are permeability and permittivity of the medium, respectively. Also, $\overline{J}_c$ is related to $\overline{E}$ as

$$\overline{J}_c = \sigma \overline{E}, \tag{2c}$$

where $\sigma$ is conductivity.

By applying (2a) through (2c) to (1a) and (1b) and arranging, it is found that

$$\mu \frac{\partial \overline{H}}{\partial t} = -\nabla \times \overline{E}, \tag{3a}$$

and

$$\varepsilon \frac{\partial \bar{E}}{\partial t} + \sigma \bar{E} = -\bar{J}_i + \nabla \times \bar{H} . \qquad (3b)$$

By using the vector identity for curl of any vectors in spherical coordinates that

$$\begin{aligned} \nabla \times \bar{A} = & \frac{\bar{a}_r}{r\sin\theta}\left[\frac{\partial}{\partial\theta}(A_\phi \sin\theta) - \frac{\partial A_\theta}{\partial\phi}\right] \\ & + \frac{\bar{a}_\theta}{r}\left[\frac{1}{\sin\theta}\frac{\partial A_r}{\partial\phi} - \frac{\partial}{\partial r}(rA_\phi)\right] \\ & + \frac{\bar{a}_\phi}{r}\left[\frac{\partial}{\partial r}(rA_\theta) - \frac{\partial A_r}{\partial\theta}\right], \end{aligned} \qquad (4)$$

in conjunction with (3a) and (3b), then separate into six field components yield

$$\mu \frac{\partial H_r}{\partial t} = \frac{1}{r\sin\theta}\left[\frac{\partial E_\theta}{\partial\phi} - \frac{\partial}{\partial\theta}(E_\phi \sin\theta)\right], \qquad (5a)$$

$$\mu \frac{\partial H_\theta}{\partial t} = \frac{1}{r}\left[\frac{\partial}{\partial r}(rE_\phi) - \frac{1}{\sin\theta}\frac{\partial E_r}{\partial\phi}\right], \qquad (5b)$$

$$\mu \frac{\partial H_\phi}{\partial t} = \frac{1}{r}\left[\frac{\partial E_r}{\partial\theta} - \frac{\partial}{\partial r}(rE_\theta)\right], \qquad (5c)$$

$$\varepsilon \frac{\partial E_r}{\partial t} + \sigma E_r = -J_r + \frac{1}{r\sin\theta}\left[\frac{\partial}{\partial\theta}(H_\phi \sin\theta) - \frac{\partial H_\theta}{\partial\phi}\right], \qquad (5d)$$

$$\varepsilon \frac{\partial E_\theta}{\partial t} + \sigma E_\theta = -J_\theta + \frac{1}{r}\left[\frac{1}{\sin\theta}\frac{\partial H_r}{\partial \phi} - \frac{\partial}{\partial r}(rH_\phi)\right], \qquad (5e)$$

$$\varepsilon \frac{\partial E_\phi}{\partial t} + \sigma E_\phi = -J_\phi + \frac{1}{r}\left[\frac{\partial}{\partial r}(rH_\theta) - \frac{\partial H_r}{\partial \theta}\right]. \qquad (5f)$$

These are the ready forms for constructing FD-TD equations by approximating the time derivatives (left hand side) and the space derivatives (right hand side) with the second (or higher) order central difference approximation. To perform the derivation, at first, the locations of the six field components must be assigned in a volume cell as illustrated in Figure 1b. This configuration is prepared for programming the FD-TD equations.

Figure 2a shows the entire problem space subdivided into many layers by constant radius spherical surfaces. The distance between two adjacent surfaces is $\Delta r$ and an index "$i$" is used to denote the constant radius surfaces. Assume that $i = 0$ at the origin ($r = 0$) and is increased by one at each outer surface and finally, $i = I_{max}$ at the outermost surface ($r = R_{max}$). Figure 2b shows the subdivided problem space by constant elevation angle ( $\theta$ ) surfaces which each is denoted by an index, "$j$". The angle is divided into $\Delta\theta$. $j = 0$ at $\theta = 0^o$ (north pole), the index is increased by one at the next $\theta$-constant surface and so on, until the final surface is reached, $j = J_{max}$ ($\theta = 180^o$, south pole). In Figure 2c, the problem space is subdivided into many volume segments in azimuth-angle ($\phi$) direction by $\phi$-constant surfaces (angle between two adjacent surfaces is $\Delta\phi$). Each surface is represented by an index "$k$". $k = 0$ at $\phi = 0^o$ (prime meridian) and stepped by one and finally, $k = K_{max}$ at $\phi = 360^o$ which is exactly the same surface at $k = 0$. In addition to the three orthogonal variables in spherical coordinates ($r$, $\theta$ and $\phi$), they are assigned to be functions of $i\,(r(i))$, $j\,(\theta(j))$ and $k\,(\phi(k))$, respectively.

Practically, aforementioned increments distance in radial direction ($\Delta r$) and angle in $\theta-$ and $\phi-$ directions ($\Delta\theta$ and $\Delta\phi$, respectively) may not be constant over the entire problem space. Thus, normally, $\Delta r$, $\Delta\theta$ and $\Delta\phi$ are considered as functions of $i(\Delta r(i))$, $j(\Delta\theta(j))$ and $k(\Delta\phi(k))$, respectively. Alternatively, if $\Delta r$, $\Delta\theta$ and $\Delta\phi$ are assigned to be constant over the entire problem space, $\Delta r(i) = \Delta r$, $\Delta\theta(j) = \Delta\theta$ and $\Delta\phi(k) = \Delta\phi$ can simply be obtained for any values of $i$, $j$ and $k$, respectively. The conventions as described above can be summarized as follows:

In *R-direction*

$$\begin{aligned} r(0) &= 0, \\ r(I_{max}) &= R_{max}, \\ \Delta r(i) &= r(i+1) - r(i). \end{aligned} \tag{6a}$$

In *θ–direction*

$$\begin{aligned} \theta(0) &= 0^{o} \\ \theta(J_{max}) &= 180^{o}, \\ \Delta\theta(j) &= \theta(j+1) - \theta(j). \end{aligned} \tag{6b}$$

In *ϕ–direction*

$$\begin{aligned} \phi(0) &= 0^{o}, \\ \phi(K_{max}) &= 360^{o}, \\ \Delta\phi(k) &= \phi(k+1) - \phi(k). \end{aligned} \tag{6c}$$

The second order central finite-difference (half-step) approximation for time and space derivatives are found to be

$$\frac{\partial f(i,j,k)^{n}}{\partial t} \approx \frac{f(i,j,k)^{n+1/2} - f(i,j,k)^{n-1/2}}{\Delta t}, \tag{7a}$$

and

$$\frac{\partial f(i,j,k)^{n}}{\partial t} \approx \frac{f(i+1/2,\ j,k)^{n} - f(i-1/2,\ j,k)^{n}}{\Delta r}, \tag{7b}$$

where $f(i, j, k)^{n} \equiv f(r(i), \theta(j), \phi(k), n\Delta t)$.

By applying (7a) and (7b) to (5d), it is found that E-field components are preferring to be considered as initial which can be written as

$$\varepsilon\frac{E_r(i,j,k)^{n+1/2}-E_r(i,j,k)^{n-1/2}}{\Delta t}+\frac{\sigma}{2}(E_r(i,j,k)^{n+1/2}+E_r(i,j,k)^{n-1/2})$$
$$=-J_r(i,j,k)^n+\frac{1}{r(i+1/2)\sin\theta(j)}$$
$$\times\left[\frac{\sin\theta(j+1/2)H_\phi(i,j+1/2,k)^n-\sin\theta(j-1/2)H_\phi(i,j-1/2,k)^n}{\Delta\theta(j-1/2)}\right.$$
$$\left.-\frac{H_\theta(i,j,k+1/2)^n-H_\theta(i,j,k-1/2)^n}{\Delta\phi(k-1/2)}\right], \qquad (8a)$$

after rearranging, the recurrence relation can be obtained as

$$E_r(i,j,k)^{n+1/2}=\frac{\varepsilon/\Delta t-\sigma/2}{\varepsilon/\Delta t+\sigma/2}E_r(i,j,k)^{n-1/2}$$
$$+\frac{1}{\varepsilon/\Delta t+\sigma/2}\left\{-J_r(i,j,k)^n+\frac{1}{r(i+1/2)\sin\theta(j)}\right.$$
$$\times\left[\frac{\sin\theta(j+1/2)H_\phi(i,j+1/2,k)^n-\sin\theta(j-1/2)H_\phi(i,j-1/2,k)^n}{\Delta\theta(j-1/2)}\right.$$
$$\left.\left.-\frac{H_\theta(i,j,k+1/2)^n-H_\theta(i,j,k-1/2)^n}{\Delta\phi(k-1/2)}\right]\right\}, \qquad (8b)$$

which (8b) is valid for $i = 0$ to $I_{max}-1$, $j = 1$ to $J_{max}-1$ and $k = 1$ to $K_{max}$.

Similarly, (5e) and (5f) can be derived to get recurrence relations, respectively, as

$$E_\theta(i,j,k)^{n+1/2} = \frac{\varepsilon/\Delta t - \sigma/2}{\varepsilon/\Delta t + \sigma/2} E_\theta(i,j,k)^{n-1/2} + \frac{1}{\varepsilon/\Delta t + \sigma/2}\left\{-J_\theta(i,j,k)^n + \frac{1}{r(i)} \times \left[\frac{H_r(i,j,k+1/2)^n - H_r(i,j,k-1/2)^n}{\sin\theta(j)\Delta\phi(k-1/2)} - \frac{r(i+1/2)H_\phi(i+1/2,j,k)^n - r(i-1/2)H_\phi(i-1/2,j,k)^n}{\Delta r(i-1/2)}\right]\right\}, \quad (8c)$$

which (8c) is valid for $i = 1$ to $I_{max}-1$, $j = 0$ to $J_{max}-1$ and $k = 1$ to $K_{max}$,

$$E_\phi(i,j,k)^{n+1/2} = \frac{\varepsilon/\Delta t - \sigma/2}{\varepsilon/\Delta t + \sigma/2} E_\phi(i,j,k)^{n-1/2} + \frac{1}{\varepsilon/\Delta t + \sigma/2}\left\{-J_\phi(i,j,k)^n + \frac{1}{r(i)} \times \left[\frac{r(i+1/2)H_\theta(i+1/2,j,k)^n - r(i-1/2)H_\theta(i-1/2,j,k)^n}{\Delta r(i-1/2)} - \frac{H_r(i,j+1/2,k)^n - H_r(i,j-1/2,k)^n}{\Delta\theta(j-1/2)}\right]\right\}, \quad (8d)$$

which (8d) is valid for $i = 1$ to $I_{max}-1$, $j = 1$ to $J_{max}-1$ and $k = 0$ to $K_{max}-1$.

Additionally, the $\sigma E$ terms in (5d) through (5f), where $\sigma$ is conductivity, can be approximated by averaging E-field components at present $(n+1/2)$ and previous $(n-1/2)$ time-step. This method is well-known as "semi-implicit approximation"[7].

Similarly, by utilizing (7a), (7b) and (5a) the results are obtained as

$$\mu \frac{H_r(i,j,k)^{n+1} - H_r(i,j,k)^n}{\Delta t}$$
$$= \frac{1}{r(i)\sin\theta(j+1/2)} \left[ \frac{E_\theta(i,j,k+1)^{n+1/2} - E_\theta(i,j,k)^{n+1/2}}{\Delta\phi(k)} \right. \quad (9a)$$
$$\left. - \frac{\sin\theta(j+1)E_\phi(i,j+1,k)^{n+1/2} - \sin\theta(j)E_\phi(i,j,k)^{n+1/2}}{\Delta\theta(j)} \right],$$

and can be rewritten to get recurrence relation

$$H_r(i,j,k)^{n+1} = H_r(i,j,k)^n$$
$$+ \frac{\Delta t}{\mu r(i)\sin\theta(j+1/2)} \left[ \frac{E_\theta(i,j,k+1)^{n+1/2} - E_\theta(i,j,k)^{n+1/2}}{\Delta\phi(k)} \right. \quad (9b)$$
$$\left. - \frac{\sin\theta(j+1)E_\phi(i,j+1,k)^{n+1/2} - \sin\theta(j)E_\phi(i,j,k)^{n+1/2}}{\Delta\theta(j)} \right],$$

which (9b) is valid for $i = 1$ to $I_{max}$, $j = 0$ to $J_{max}-1$ and $k = 0$ to $K_{max}-1$.

Similarly, by applying (7a) and (7b) to (5b) and (5c) and after rearranging yields,

$$H_\theta(i,j,k)^{n+1} = H_\theta(i,j,k)^n$$
$$+ \frac{\Delta t}{\mu r(i+1/2)} \left[ \frac{r(i+1)E_\phi(i+1,j,k)^{n+1/2} - r(i)E_\phi(i,j,k)^{n+1/2}}{\Delta r(i)} \right. \quad (9c)$$
$$\left. - \frac{E_r(i,j,k+1)^{n+1/2} - E_r(i,j,k)^{n+1/2}}{\sin\theta(j)\Delta\phi(k)} \right],$$

which (9c) is valid for $i = 0$ to $I_{max}-1$, $j = 0$ to $J_{max}-1$ and $k = 0$ to $K_{max}-1$,

$$H_\phi(i,j,k)^{n+1} = H_\phi(i,j,k)^n + \frac{\Delta t}{\mu r(i+1/2)}\left[\frac{E_r(i,j+1,k)^{n+1/2} - E_r(i,j,k)^{n+1/2}}{\Delta\theta(j)} - \frac{r(i+1)E_\theta(i+1,j,k)^{n+1/2} - r(i)E_\theta(i,j,k)^{n+1/2}}{\Delta r(i)}\right], \quad (9d)$$

which (9d) is valid for $i = 0$ to $I_{max}-1$, $j = 0$ to $J_{max}-1$ and $k = 0$ to $K_{max}-1$.

In addition, for (8a) through (9d), $\varepsilon$'s and $\mu$'s should be the values at which fields are to be determined.

## Singularities considerations

The singularities of the space grid will be considered and treated in this section. By means of the finite-difference approximation of the electromagnetic field in each components as formulated in (8b)-(8d) and (9b)-(9d), respectively, the indices $i$, $j$ and $k$ have their own valid intervals such as the index $j$ in (8b) can be run from $1$ to $J_{max}-1$ only. The points where the algorithm cannot be advanced as usual ways (using (8b) through (9d)) are referred to as "singularities". There are three main singularities occur in the 3D FD-TD. Typically, some singular points can be treated to find some field components and others cannot.

The first singularity occurs at the prime meridian which is on the $\phi$-constant surface at $\phi = 0^o$ and $360^o$ as shown in Figure 3a. From (8b) through (9d), it is evident that all of the six field components are affected by this singularity. If the index $k$ is run from $0$ to $K_{max}$, the field components at this surface will be calculated twice. This problem can be treated by means of "joining conditions"[4] which can be derived directly from (8b) through (9d) as

$$E_r(i, j, 0)^{n+1/2} = E_r(i, j, K_{max})^{n+1/2}, \quad (10a)$$

$$E_\theta(i, j, 0)^{n+1/2} = E_\theta(i, j, K_{max})^{n+1/2}, \quad (10b)$$

$$E_\phi(i, j, K_{max})^{n+1/2} = E_\phi(i, j, 0)^{n+1/2}, \quad (10c)$$

$$H_r(i, j, K_{max})^{n+1} = H_r(i, j, 0)^{n+1}, \quad (10d)$$

$$H_\theta(i, j, K_{max})^{n+1} = H_\theta(i, j, 0)^{n+1}, \quad (10e)$$

$$H_\phi(i, j, K_{max})^{n+1} = H_\phi(i, j, 0)^{n+1}. \quad (10f)$$

The second singularity which is more difficult to treat occurs at the north ($\theta = 0^o$) and south ($\theta = 180^o$) poles as shown in Figure 3b. Evidently, there are three field components (e.g. $E_r$, $E_\phi$ and $H_\theta$) gathered in these poles. Presently, only the $E_r$ field component can be approximated (the $E_\phi$ and $H_\theta$ are simply set to be zero). By utilizing the integral form of the curl $\bar{H}$ equation[4]

$$\int_C \bar{H} \cdot d\bar{l} = \iint (\bar{J}_i + \sigma\bar{E} + \varepsilon \frac{\partial \bar{E}}{\partial t}) \cdot d\bar{A}, \quad (11a)$$

where $\int_C$ denotes integral along closed-path $C$ and then recast (11a) into an approximated form as

$$\frac{\int_C \bar{H} \cdot d\bar{l}_{\Delta A}}{\Delta A} \approx (\bar{J}_i + \sigma\bar{E} + \varepsilon \frac{\partial \bar{E}}{\partial t})_N, \quad (11b)$$

where the $\Delta A$ subscript of $d\bar{l}$ indicates that the differential path which is the perimeter of the differential area $\Delta A$, and the subscript $N$ denotes the right-hand normal to $\Delta A$, as show in Figure 3c.

By applying (7a) to the right side of (11b) and rearranging yields

$$E_r(i,j,k)^{n+1/2} = \frac{\varepsilon/\Delta t - \sigma/2}{\varepsilon/\Delta t + \sigma/2} E_r(i,j,k)^{n-1/2} + \frac{1}{\varepsilon/\Delta t + \sigma/2}\left\{ -J_r(i,j,k)^n + \frac{\int_C H_\varphi \cdot dl_{\Delta A}}{\Delta A} \right\}. \qquad (11c)$$

For the north pole $(j = 0)$, the closed-path $C$ is defined by the $\theta(1/2)$-circle on $r(i+1/2)$-surface as depicted in Figure 3b. The integral term of (11c) can be approximated by a summation of products of $H_\phi$ and $d\bar{l}_{\Delta A}$ as

$$\int_C H_\phi \cdot dl_{\Delta A} \approx \sum_{k=0}^{K_{max}-1} H_\phi r(i+1/2)\sin\theta(1/2)\Delta\phi(k), \qquad (11d)$$

and the differential area $\Delta A$ is replaced by the area on the $r(i+1/2)$-surface bounded by the closed-path $C$

$$\Delta A = \int_0^{2\pi}\int_0^{\theta(1/2)} r^2(i+1/2)\sin\theta \, d\theta d\phi = 2\pi r^2(i+1/2)\left[1-\cos\theta(1/2)\right]. \qquad (11e)$$

Finally, by substituting (11d) and (11e) into (11c), one obtains

$$E_r(i,j,k)^{n+1/2} = \frac{\varepsilon/\Delta t - \sigma/2}{\varepsilon/\Delta t + \sigma/2} E_r(i,j,k)^{n-1/2} + \frac{1}{\varepsilon/\Delta t + \sigma/2}\left\{ -\frac{J_r(i,j,k)^n}{} + \frac{\sin\theta(1/2)}{2\pi r(i+1/2)\left[1-\cos\theta(1/2)\right]} \sum_{k=0}^{K_{max}-1} H_\phi \Delta\phi(k) \right\}. \qquad (12)$$

Similarly, for the south pole, the closed-path $C$ is defined by the $\theta\,(J_{max}-1/2)$-circle on the $r\,(i+1/2)$-surface as in Figure 3c. By following the above procedures, one obtains

$$E_r(i,j,k)^{n+1/2} = \frac{\varepsilon/\Delta t-\sigma/2}{\varepsilon/\Delta t+\sigma/2}E_r(i,j,k)^{n-1/2} + \frac{1}{\varepsilon/\Delta t+\sigma/2}\left\{-\frac{J_r(i,j,k)^n}{2\pi r(i+1/2)\left[1+\cos\theta(J_{max}-1/2)\right]}\sum_{k=0}^{K_{max}-1}H_\phi\Delta\phi(k)\right\}. \qquad (13)$$

The third singular point takes place at the origin, as shown in Figure 3d. Because of the pyramidal shapes of the volume cells, the three field components $E_\theta$, $E_\phi$ and $H_r$ merged into the origin. So the algorithm cannot be advanced at these cells as usual ways and thus, limits utilities itself. There are some possible schemes which can be used to treat this problem such as defining a new style of finite difference approximation (e.g. *forward or backward-difference*) or assuming a perfect conductor of finite radius at the origin. Conclusively, the first singularity may reduce accuracy of the algorithm and the second scheme, sometimes causes severe reflections and leads to instability.

## Outer boundary conditions

Besides described before in the part of singularities, the outermost (truncated) boundary is another surface where the algorithm cannot be advanced as usual. So some schemes are needed to approximated the field components (e.g. $E_\theta$ and $E_\phi$) at this surface and simulate outgoing waves by reducing reflections as less as possible. These schemes are known as "absorbing boundary conditions (ABCs)" or "radiation boundary conditions (RBCs)"[7]. The method that is simple for implementing in spherical coordinates is derived in this section.

Assume that any outgoing waves can be represented in a form

$$U = \frac{f(t - r/v)}{r}, \tag{14}$$

where $U$ denotes any outgoing waves, $t$ is time, $r$ is radial distance from a reference point or an origin and $v$ is phase velocity of waves.

Here, only E-field components ($E_\theta$ and $E_\phi$) are enforced by (14) at the truncated boundary. $E$ is used instead of $U$ and the left parameters to be written in forms of the conventional parameters as defined before, so

$$E(i,j,k)^{n+1/2} = \frac{f\left[(n+1/2)\Delta t - r(i)/v\right]}{r(i)}. \tag{14a}$$

Furthermore, by using (14a) at the truncated (outermost) boundary, one obtains

$$E(I_{max},j,k)^{n+1/2} = \frac{f\left[(n+1/2)\Delta t - r(I_{max})/v\right]}{r(I_{max})}. \tag{14b}$$

As mentioned before that E-field components at the outermost boundary cannot be advanced by the algorithm, so they have to be approximated by using some known values of E-field components at an inner layer. The wisest concept is to use E-field components at the inner surface adjacent to it such as $E(I_{max}-1,\ j,\ k)^{n-1/2}$, $E(I_{max}-1,\ j,\ k)^{n-1/2}$ and (14a) can be represented in form of

$$E(I_{max}-1,j,k)^{(n-1/2)-\beta} = \frac{f\left[(n-1/2)\Delta t - r(I_{max}-1)/v - \beta\Delta t\right]}{r(I_{max}-1)}, \tag{14c}$$

where $\beta$ denotes previous time steps of $E(I_{max}-1,\ j,\ k)^{n-1/2}$ which is usually an integer value. For example, $\beta = -1$ means the present time step $E(I_{max}-1,\ j,\ k)^{n+1/2}$. Also, $E(I_{max}\ 1,\ k)^{n+1/2}$ can be written in a similar form of (14c) as

$$E(I_{max}, j, k)^{n+1/2} = \frac{f\left[(n-1/2)\Delta t - r(I_{max}-1)/v + \tau\Delta t\right]}{r(I_{max})}, \qquad (14d)$$

where $\tau = 1 - \dfrac{\left[r(I_{max}) - r(I_{max}-1)\right]}{v\Delta t} = 1 - \dfrac{\left[\Delta r(I_{max}-1)\right]}{v\Delta t}$.

From (14c) and (14d), it is clear that the arguments in both functions, $f$, are in a similar form where $-\beta$ and $\tau$ are equivalence. If $E(I_{max}-1,\ j,\ k)^{n-1/2}$ can be described by (14c), it can also describe (approximate) $E(I_{max},\ j,\ k)^{n+1/2}$ by utilizing the known values of $E(I_{max}-1,\ j,\ k)^{n-1/2}$ and (14d). $\beta$ will be chosen in order to make $f$'s in (14c) and (14d) interpolate with time (e.g. the biggest value of $\beta$ should be greater or equal to $\tau$ as shown in Figure 4). Sometimes, a value of $\tau$ may be very large. From (14c) and (14d), it is evident that the arguments of $f$'s are similar, except the terms $-\beta\Delta t$ and $\tau\Delta t$ so $f$'s can be described as follows:

$$f((n-1/2)\Delta t - r(I_{max}-1)/v - \beta\Delta t) \equiv f((n-1/2)\Delta t - r(I_{max}-1)/v + \tau\Delta t) \equiv f(u), \qquad (14e)$$

where $u$ can be either $-\beta\Delta t$ or $\tau\Delta t$. Thus, $E(I_{max}-1,\ j,\ k)^{n-1/2-\beta}$ and (14c) can be used for approximating $E(I_{max},\ j,\ k)^{n-1/2}$ at the outer boundary. The constant $\beta$ can be selected to have different styles of approximations (e.g. interpolations or extrapolations) and the function $f$'s often be chosen to have the order of accuracy equal to the algorithm's. Here, the central finite-difference approximation, which is the second-order of accuracy is used, so the second-order polynomials are chosen for $f$'s (the higher order

polynomials may yield more accurate results but stabilities of FD–TD algorithms will be very rapidly degraded)

$$f(u) = A + Bu + Cu^2, \tag{14f}$$

where $A$, $B$ and $C$ are coefficients to be determined.

In order to interpolate $E(I_{max}, j, k)^{n+1/2}$ by the known field values, $E(I_{max}-1, j, k)^{n-1/2-\beta}$ three equations, which recasted from (14c), are needed to be solved simultaneously in conjunction with the convention in (14e)

$$f(-\beta_1\Delta t) = A - B\beta_1\Delta t + C(\beta_1\Delta t)^2 = r(I_{max}-1)E(I_{max}-1, j, k)^{n-1/2-\beta_1}, \tag{15a}$$

$$f(-\beta_2\Delta t) = A - B\beta_2\Delta t + C(\beta_2\Delta t)^2 = r(I_{max}-1)E(I_{max}-1, j, k)^{n-1/2-\beta_2}, \tag{15b}$$

and

$$f(-\beta_3\Delta t) = A - B\beta_3\Delta t + C(\beta_3\Delta t)^2 = r(I_{max}-1)E(I_{max}-1, j, k)^{n-1/2-\beta_3}. \tag{15c}$$

The constants $\beta_1$, $\beta_2$ and $\beta_3$ must be chosen as shown in Figure 4 such that $\beta_1 v\Delta t$ should be at $I_{max}-1$ (or inner) surface, $\beta_3 v\Delta t$ should be at $I_{max}$ (or outer) surface and $\beta_2 v\Delta t$ is between these two surfaces. Typical values for $\beta_1$, $\beta_2$ and $\beta_3$ (in case of $\Delta r/2v\Delta t = 1$) are $-1$, $0$ and $1$, respectively, which yield an interpolation with time. In spherical coordinates, sometimes the ratio $\Delta r/2v\Delta t$ is much greater than $1$ (typically, exceeds ten times, so as $\beta_3$) that leads to inaccurate results. So, one may need less stable, but easy to implement, extrapolations by using $\beta_1 = -1$, $\beta_2 = 0$ and $\beta_3 = 1$ and doing the extrapolation for every time steps.

Once the coefficients $A$, $B$ and $C$ are determined [from (15a) to (15c)] $E(I_{max}\, j, k)^{n+1/2}$ can be found by applying (14f) to (14d)

$$E(I_{max}, j,k)^{n+1/2} = \frac{f(\tau\Delta t)}{r(I_{max})}. \qquad (16)$$

Another alternative way is to use linear (first-order polynomial) interpolations which simply utilizing a distance ratio, $r(I_{max}-1)/r(I_{max})$, but additional (not excessive) computers' storage spaces are needed to store each of the E-field components (e.g. $E_\theta$ and $E_\phi$) for about $\Delta r/v\Delta t$ time steps in the past. If $N = \Delta r/v\Delta t$, $E(I_{max}, j, k)^{n+1/2}$ can be approximated by using the $(N-1)th$ values of the stored $E(I_{max}-1, j, k)^{n+1/2}$ in the past

$$E(I_{max}, j,k)^{n+1/2} = \frac{r(I_{max}-1)E_{(N-1)}(I_{max}-1, j,k)^{n+1/2}}{r(I_{max})}, \qquad (17)$$

where the subscript $(N-1)$ indicates the $(N-1)th$ stored values of $E(I_{max}-1, j, k)^{n+1/2}$ in the past.

## Stability criterion for 3D FD-TD in spherical coordinates

The objective of deriving a stability criterion is to have a guiding rule for determining a time step, $\Delta t$, which maintains an algorithm's stability throughout a program run. A stability criterion takes different form for different coordinate systems. Here, a derived stability criterion is used for a nonorthogonal curvilinear FD-TD algorithm to derive a stability criterion for 3D spherical coordinates.

A stability criterion for nonorthogonal curvilinear coordinates is found to be[7]

$$\Delta t \le \frac{1}{c}\sqrt{\frac{g^{i,j}}{\sum_{i=1}^{3}\sum_{j=1}^{3}\Delta u^i \Delta u^i}}, \qquad (18a)$$

where $g^{i,j}$ is an inverse metric tensor of a metric tensor $g_{i,j}$ and $\Delta u$'s are increments in directions of coordinate parameters.

In spherical coordinates, and other orthogonal coordinates, $g^{i,j} = g^{i,i} = 1/g^{i,i} = 1/(h_i)^2$ for $i \neq j$ and $g^{i,j} = 0$ for $i = j$. By substituting $\Delta u^1 = \Delta r$, $\Delta u^2 = \Delta\theta$, $\Delta u^3 = \Delta\phi$, $h_1 = 1$, $h_2 = r$ and $h_3 = r\sin\theta$ into (18a), one obtains

$$\Delta t \leq \frac{1}{c\sqrt{\frac{1}{(\Delta r)^2} + \frac{1}{(r\Delta\theta)^2} + \frac{1}{(r\sin\theta\Delta\phi)^2}}}. \qquad (18b)$$

Because of its behavior depends on $r$ and $\theta$ as shown in Figure 5, all parameters in (18b) must be determined from the smallest volume cell in problem space. However, the upper limit of $\Delta t$ can be calculated from (18b) may not last stability of algorithms very long. Practically, $\Delta t$ (upper limit) is divided by some constant factors such as 5 or 10, or use one-half of increments (e.g. $\Delta t/2$, $\Delta\theta/2$ and $\Delta\phi/2$) in (18b) to ensure stability.

## NUMERICAL RESULTS

There are two problems considered here. Firstly, same configurations as in Holland[4], with pulse sources (Gaussian), are repeated, except that the extrapolating and linear radiation boundary conditions as formulated before are implemented. Then, new configurations of problems are considered by applying continuous sources such as infinitesimal electric and magnetic dipoles.

In first problem, the Gaussian pulse source is used, which is defined as

$$\bar{f}(r;t) = \bar{a}_i I_o \exp\left[\frac{-(t - r/v - t_o)^2}{\sigma^2}\right], \qquad (19a)$$

where $\bar{a}_i$, $I_o$, $t_o$ and $\sigma$ are unit vector, amplitude, time delay and pulsewidth, respectively.

Considering an electric dipole is aligned along $z$-axis at the origin, and the configurations of parameters are as follows: $R_{max} = 10m$, $\Delta r = 0.5m$ $(I_{max} = 20)$; $\Delta\theta = \pi/12$ $(15^o, J_{max} = 12)$ ; $\Delta\phi = \pi/9$ $(20^o, K_{max} = 18)$ and $\sigma = 2 \times 10^{-8}$. The corresponding electric field components are found to be[4]

$$E_r = \frac{\cos\theta}{2\pi\varepsilon_o}\left[\frac{f'(t-r/v)}{r^2 v} + \frac{f(t-r/v)}{r^2}\right], \qquad (19b)$$

$$E_\theta = \frac{\sin\theta}{4\pi\varepsilon_o}\left[\frac{f''(t-r/v)}{rv^2} + \frac{f'(t-r/v)}{r^2 v} + \frac{f(t-r/v)}{r^3}\right], \qquad (19c)$$

where $f'$ and $f''$ represent first and second derivatives of $f$, respectively. By applying (19c) as electric-field boundary condition for $E_\theta$ in the algorithm at $i = 4$ $(r = 2m)$, $\Delta t \cong 1.85 \times 10^{-11}$ $sec$ [from (18b)] and using $t_o = 6 \times 10^{-8}$ sec, the results are shown in Figure 6a and 6b at $r = 10m$ $(i = I_{max})$ and $\theta = 97.5^o$. In Figure 6a and 6b, a second-order extrapolating and a linear interpolating RBCs, respectively, have been used which are shown by the dash lines, labeled *no spacing cell.* It is evident that both alternative RBCs yield similar results (slightly different) and comparable with those in Holland[4] using second-order interpolating RBCs. Furthermore, the effects of RBCs have been shown on results by adding *10* and *20* spacing cells between an $i = 20$ surface (where the results are detected) and a RBC surface (where extrapolations and interpolations are calculated). It is seen in Figure 6a and 6b that the further approximating RBCs are taken away, the better results may

be achieved (but it should be noted that increasing spacing cells more than 20 ($I_{max}$) will not yield much better results). In case of magnetic dipole, the corresponding electric field component is found to be[4]

$$E_\phi = -\frac{\sin\theta}{4\pi r}\left[\frac{f''^*(t-r/v)}{v}+\frac{f'^*(t-r/v)}{r}\right], \qquad (19d)$$

where $f'^*$ and $f''^*$ are complex conjugates of first and second derivatives of $f$, respectively. By applying (19d) as electric-field boundary condition for $E_\phi$ in the algorithm and using the same values of parameters as defined before, the results are obtained as shown in Figure 7a and 7b. Again, a second-order extrapolating and a linear interpolating RBCs are utilized and yielded results in Figure 7a and 7b, respectively. Effects of RBCs on results can be concluded as in case of electric dipole. Evidently, the algorithm behaves better for case of magnetic dipole.

In the second problem, continuous wave sources are applied by utilizing equations derived for an infinitesimal dipole. A corresponding electric-field excited by current source as

$$\bar{I} = \bar{a}_z I_o \cos(\omega t). \qquad (20a)$$

In $\theta-$ direction, $E_\theta$, is found to be[1]

$$E_\theta = \frac{I_o d\eta \sin\theta}{4\pi r}\left[\frac{\cos\omega(t-r/v)}{r}+\frac{k\sin\omega(t-r/v)}{r^2}-\frac{\sin\omega(t-r/v)}{k}\right], \qquad (20b)$$

where $d$, $\eta$ and $k$ are, respectively, length of a dipole, wave impedance and wave number (phase constant). It can choose to operate at the frequency of $30\ MHz$ and use $I_o = 40\pi\ r/d\eta$. The values of parameters are $R_{max} = 40m$, $\Delta r = 1m$ ($I_{max} = 40$), $\Delta\theta = \pi/12$ ($15^o$, $J_{max} = 12$) and $\Delta\phi = \pi/9$ ($20^o$, $K_{max} = 18$). By applying (20b) in the algorithm as boundary condition for the field component, $E_\theta$, yields results as shown in Figure 8a (at $r = 40m$ and $\theta = 97.5^o$). For case of infinitesimal magnetic dipole, the corresponding electric-field, $E_\phi$, produced is[1]

$$E_\phi = -\frac{I_o d\eta \sin\theta}{4\pi r}\left[\frac{\cos\omega(t - r/v)}{r} - k\sin\omega(t - r/v)\right]. \qquad (20c)$$

The same procedures as in the infinitesimal electric dipole are done for case of infinitesimal magnetic dipole, using the same values of the parameters by applying (20c) to the algorithm as boundary condition for the field component, $E_\phi$, yields results as shown in Figure 8b. As seen in Figure 8a and 8b, both electric and magnetic dipole have the similar behaviors when compare with their exact solutions. Furthermore, some spacing cells are added (results are not shown here) and used in different types of RBCs like in the first problem, the results are not much better than that shown in Figure 8a and 8b which are no spacing cell added.

## CONCLUSIONS

This paper has shown rigorous formulations of the 3D FD-TD. The derivation is started by constructing finite-difference approximation from Maxwell's equations and each point in the spherical volume cell is assigned its locations for

programming. The three main singularities, which occur in $R$, $\theta$ and $\phi$-direction, are treated. Some alternative ways are used to frequency approximate the electric field components at the truncated surface by means of the second-order polynomial extrapolating and linear interpolating RBCs. From the numerical results, the two alternative ways yield good approximations at the truncated surface when compared with the previous work[4]. Also, it can conclude that problems involving magnetic dipole sources behaved better than those of electric dipole sources, as concluded in Holland[4], but this may be true for cases of pulse sources, only. Alternatively, in cases of continuous sources (infinitesimal dipoles), it is not observable that the problem involving the magnetic dipole source behaved better than that one of the electric dipole source. By this reason, it can conclude that continuous wave sources are immune to certain types of RBCs. Effects of simulating RBCs on calculating field components in cases of pulse sources are more serious than those in cases of continuous sources, but in cases of pulse sources, results can be improved by adding spacing cells whereas in events of continuous sources cannot. The stability criterion for the 3D FD-TD algorithms in spherical coordinates is derived from the criterion of the nonorthogonal coordinates. Ultimately, it has been suggested that using one-halves of the increments (e.g. $\Delta t/2$, $\Delta\theta/2$ and $\Delta\phi/2$) yields goods stability.

## ACKNOWLEDGEMENTS

The authors deeply appreciate the kindness discussion of Prof. Toshio Wakabayashi from Tokai University. This work was supported by the National Science and Technology Development Agency (NSTDA) under the career development award and local graduate scholarship program.

# REFERENCES


1. Balanis, C.A. Antenna Theory Analysis and Design. John Wiley & Sons, 1982, 100–103, 164–169.
2. Holland, R. THREDS: A Free–field EMP Coupling and Scattering Code. *IEEE Trans. Nucl. Sci.*, 1977, **NS-24**, 2416–2421.
3. Holland, R., Simpson, L. and Kunz, K.S. Finite–difference Analysis of EMP Coupling to Lossy Dielectric Structures. *IEEE Trans. Electromagn. Compat.*, Aug. 1980, **EMC-22**, 203–209.
4. Holland, R. THREDS: A Finite–difference Time–domain EMP Code in 3D Spherical Coordinates. *IEEE Trans. Nucl. Sci., Dec. 1983*, **NS-30**, 4592–4595.
5. Joseph, R.M. and Taflove, A. FD–TD Maxwell's Equations Models for Nonlinear Electrodynamics and Optics. *IEEE Trans. Antennas & Prop., Mar. 1997*, **AP-45**, 364–374.
6. Taflove, A. and Brodwin, M.E. Numerical Solution of Steady–state Electromagnetic Scattering Problems Using the Time–dependent Maxwell's Equations. *IEEE Trans. Microwave Theory Tech.*, Aug. 1975, **MTT-23**, 623–630.
7. Taflove, A. Computational Electrodynamics the Finite–difference Time–domain Method. Artech House, 1995, 353–361.
8. Umashankar, K. and Taflove, A. A Novel Method to Analyze Electromagnetic Scattering of Complex Objects. *IEEE Trans. Electromagn. Compat.*, Nov. 1982, **EMC-24**, 397–405.
9. Yee, K.S. Numerical Solution of Initial Boundary Value Problems Involving Maxwell's Equations in Isotropic Media. *IEEE Trans. Ant. & Prop.*, May 1966, **AP-14**, 302–307.

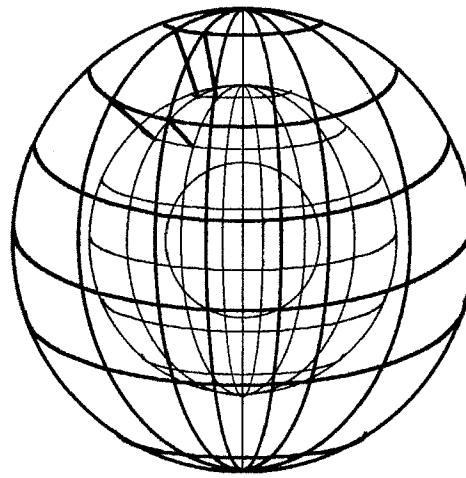

**Fig. 1a Geometry of the problem**

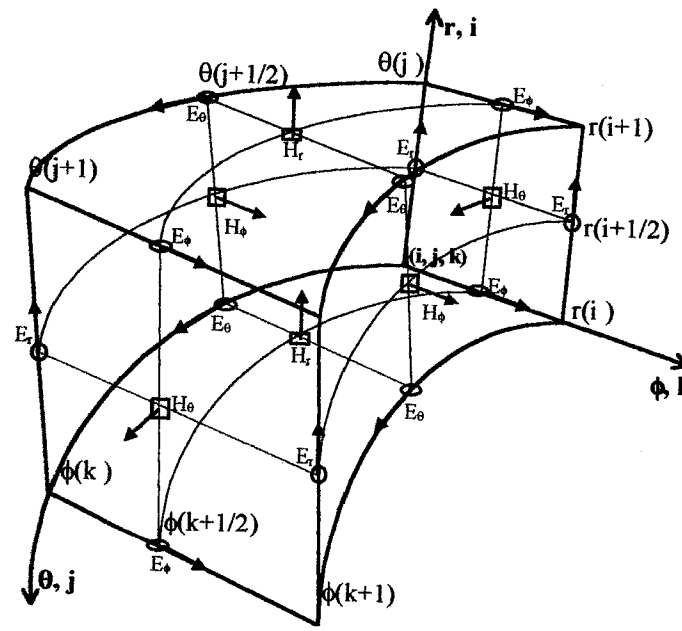


**Fig. 1b Locations of the field components on a volume cell**

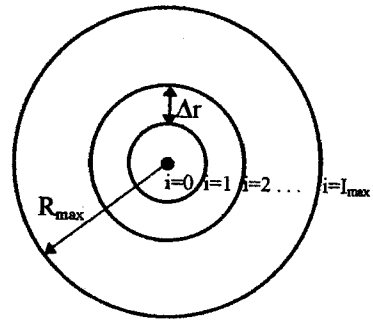


**Fig. 2a Subdivisions of the problem space in the radial direction**

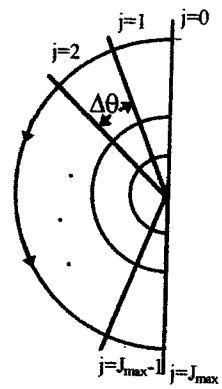


**Fig. 2b Subdivisions of the problem space in the $\theta$ - direction**

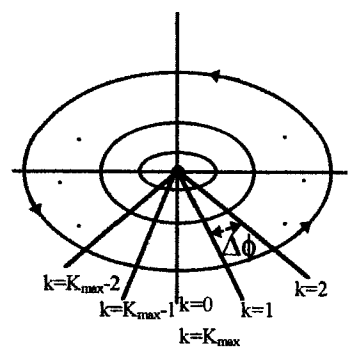


**Fig. 2c Subdivisions of the problem space in the $\phi$ - direction**

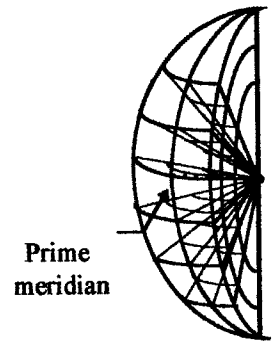


**Fig. 3a The first singularity, $K=1$ and $N\phi$**

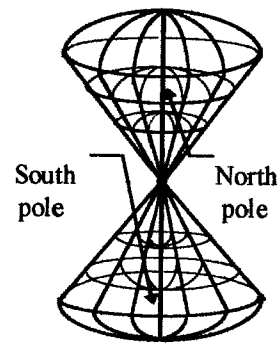


**Fig. 3b The second singularity**

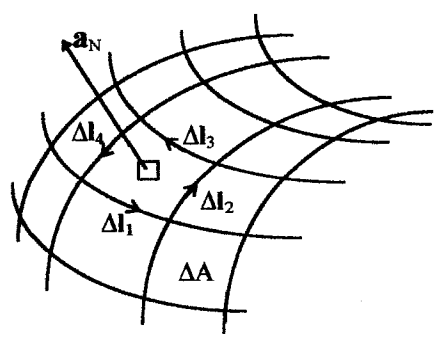


**Fig. 3c The differential area ($\Delta A$) enclosed by the differential paths ($\Delta l$)**

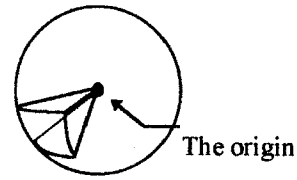


**Fig. 3d The third singularity**

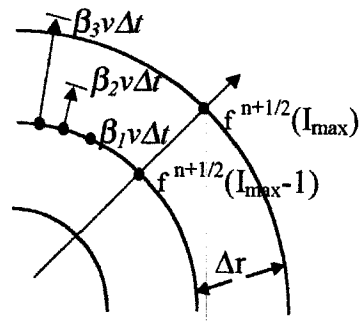


**Fig. 4 Locations of $f^{n+1/2}(I_{max})$ and $f^{n+1/2}(I_{max}-1)$**

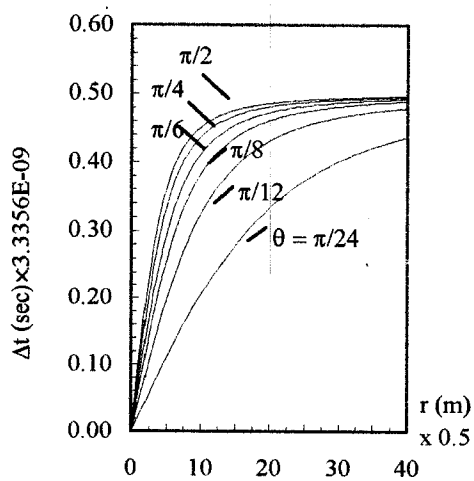


**Fig. 5 Variation of $\Delta t$ as a function of $r$**

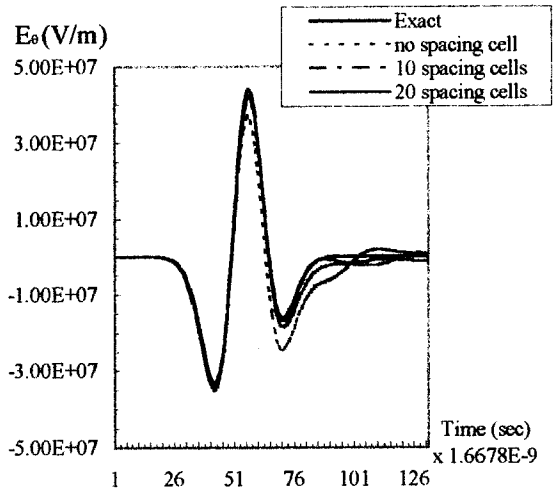


**Fig. 6a** **Electric dipole (Gaussian pulse)**
**2nd-order extrapolating RBC at r=20m θ = 97.5°**

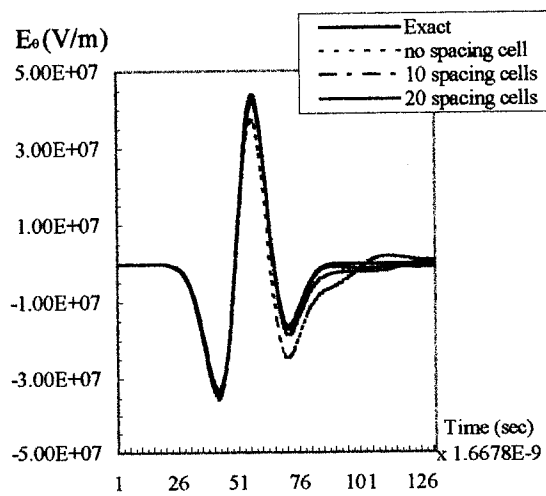


**Fig. 6b** **Electric dipole (Gaussian pulse)**
**linear interpolating RBC at r=20m θ =97.5°**

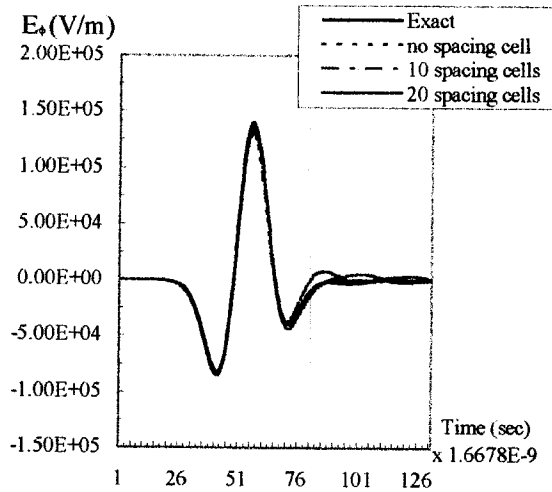


**Fig. 7a Magnetic dipole (Gaussian pulse)**
**2nd-order extrapolating RBC at r=20m θ =90°**

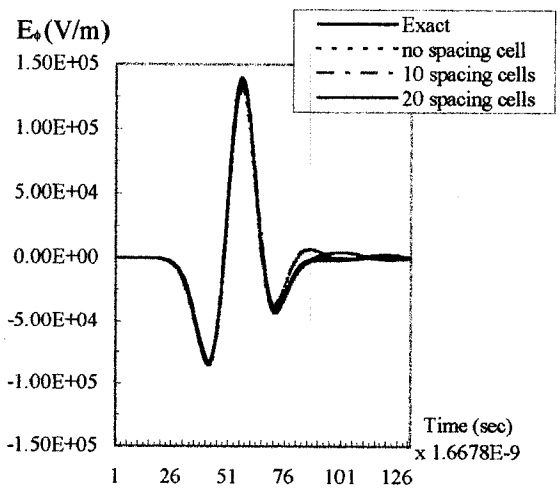


**Fig. 7b Magnetic dipole (Gaussian pulse)**
**linear interpolating RBC at r=20m θ =90°**

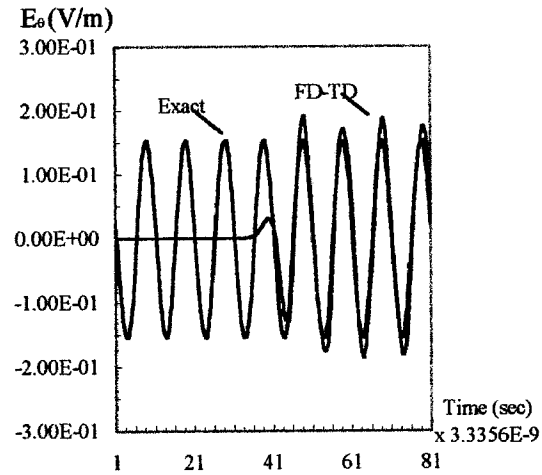


**Fig. 8a Infinitesimal electric dipole at r=40m θ =97.5°**

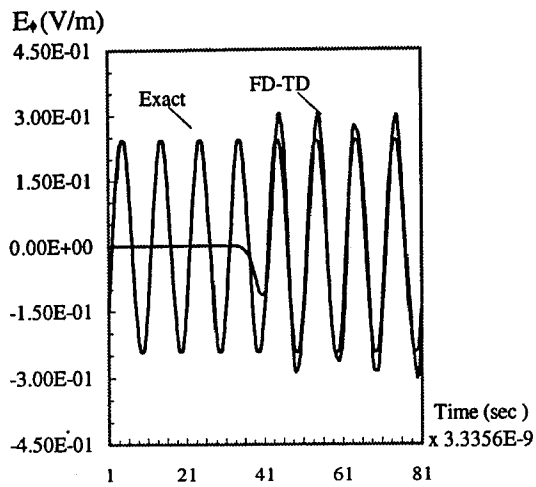


**Fig. 8b Infinitesimal magnetic dipole at r=40m θ =90°**